Search for squark production in R-parity violating supersymmetry at HERA

Eur. Phys. J. C 36, 425–440 (2004)
Digital Object Identifier (DOI) 10.1140/epjc/s2004-01982-2

THE EUROPEAN PHYSICAL JOURNAL C

Search for squark production in R-parity violating supersymmetry at HERA

The H1 Collaboration

A. Aktas[10], V. Andreev[26], T. Anthonis[4], A. Asmone[33], A. Babaev[25], S. Backovic[37], J. Bähr[37], P. Baranov[26], E. Barrelet[30], W. Bartel[10], S. Baumgartner[38], J. Becker[39], M. Beckingham[21], O. Behnke[13], O. Behrendt[7], A. Belousov[26], Ch. Berger[1], N. Berger[38], T. Berndt[14], J.C. Bizot[28], J. Böhme[10], M.-O. Boenig[7], V. Boudry[29], J. Bracinik[27], V. Brisson[28], H.-B. Bröker[2], D.P. Brown[10], D. Bruncko[16], F.W. Büsser[11], A. Bunyatyan[12,36], G. Buschhorn[27], L. Bystritskaya[25], A.J. Campbell[10], S. Caron[1], F. Cassol-Brunner[22], K. Cerny[32], V. Chekelian[27], C. Collard[4], J.G. Contreras[23], Y.R. Coppens[3], J.A. Coughlan[5], M.-C. Cousinou[22], B.E. Cox[21], G. Cozzika[9], J. Cvach[31], J.B. Dainton[18], W.D. Dau[15], K. Daum[35,41], B. Delcourt[28], R. Demirchyan[36], A. De Roeck[10,44], K. Desch[11], E.A. De Wolf[4], C. Diaconu[22], J. Dingfelder[13], V. Dodonov[12], A. Dubak[27], C. Duprel[2], G. Eckerlin[10], V. Efremenko[25], S. Egli[34], R. Eichler[34], F. Eisele[13], M. Ellerbrock[13], E. Elsen[10], M. Erdmann[10,42], W. Erdmann[38], P.J.W. Faulkner[3], L. Favart[4], A. Fedotov[25], R. Felst[10], J. Ferencei[10], M. Fleischer[10], P. Fleischmann[10], Y.H. Fleming[3], G. Flucke[10], G. Flügge[2], A. Fomenko[26], I. Foresti[39], J. Formánek[32], G. Franke[10], G. Frising[1], E. Gabathuler[18], K. Gabathuler[34], E. Garutti[10], J. Garvey[3], J. Gayler[10], R. Gerhards[10,†], C. Gerlich[13], S. Ghazaryan[36], L. Goerlich[6], N. Gogitidze[26], S. Gorbounov[37], C. Grab[38], H. Grässler[2], T. Greenshaw[18], M. Gregori[19], G. Grindhammer[27], C. Gwilliam[21], D. Haidt[10], L. Hajduk[6], J. Haller[13], M. Hansson[20], G. Heinzelmann[11], R.C.W. Henderson[17], H. Henschel[37], O. Henshaw[3], R. Heremans[4], G. Herrera[24], I. Herynek[31], R.-D. Heuer[11], M. Hildebrandt[34], K.H. Hiller[37], J. Hladký[31], P. Höting[2], D. Hoffmann[22], R. Horisberger[34], A. Hovhannisyan[36], M. Ibbotson[21], M. Ismail[21], M. Jacquet[28], L. Janauschek[27], X. Janssen[10], V. Jemanov[11], L. Jönsson[20], D.P. Johnson[4], H. Jung[20,10], D. Kant[19], M. Kapichine[8], M. Karlsson[20], J. Katzy[10], N. Keller[39], J. Kennedy[18], I.R. Kenyon[3], C. Kiesling[27], M. Klein[37], C. Kleinwort[10], T. Kluge[1], G. Knies[10], A. Knutsson[20], B. Koblitz[27], V. Korbel[10], P. Kostka[37], R. Koutouev[12], A. Kropivnitskaya[25], J. Kroseberg[39], J. Kückens[10], T. Kuhr[10], M.P.J. Landon[19], W. Lange[37], T. Laštovička[37,32], P. Laycock[18], A. Lebedev[26], B. Leißner[1], R. Lemrani[10], V. Lendermann[14], S. Levonian[10], L. Lindfeld[39], K. Lipka[37], B. List[38], E. Lobodzinska[37,6], N. Loktionova[26], R. Lopez-Fernandez[10], V. Lubimov[25], H. Lueders[11], D. Lüke[7,10], T. Lux[11], L. Lytkin[12], A. Makankine[8], N. Malden[21], E. Malinovski[26], S. Mangano[38], P. Marage[4], J. Marks[13], R. Marshall[21], M. Martisikova[10], H.-U. Martyn[1], S.J. Maxfield[18], D. Meer[38], A. Mehta[18], K. Meier[14], A.B. Meyer[11], H. Meyer[35], J. Meyer[10], S. Michine[26], S. Mikocki[6], I. Milcewicz[6], D. Milstead[18], A. Mohamed[18], F. Moreau[29], A. Morozov[8], I. Morozov[8], J.V. Morris[5], M.U. Mozer[13], K. Müller[39], P. Murín[16,43], V. Nagovizin[25], B. Naroska[11], J. Naumann[7], Th. Naumann[37], P.R. Newman[3], C. Niebuhr[10], A. Nikiforov[27], D. Nikitin[8], G. Nowak[6], M. Nozicka[32], R. Oganezov[36], B. Olivier[10], J.E. Olsson[10], G.Ossoskov[8], D. Ozerov[25], C. Pascaud[28], G.D. Patel[18], M. Peez[29], E. Perez[9], A. Perieanu[10], A. Petrukhin[37], D. Pitzl[10], R. Placakyte[27], R. Pöschl[10], B. Portheault[28], B. Povh[12], N. Raicevic[37], Z. Ratiani[10], P. Reimer[31], B. Reisert[27], A. Rimmer[18], C. Risler[27], E. Rizvi[3], P. Robmann[39], B. Roland[4], R. Roosen[4], A. Rostovtsev[25], Z. Rurikova[27], S. Rusakov[26], K. Rybicki[6,†], D.P.C. Sankey[5], E. Sauvan[22], S. Schätzel[13], J. Scheins[10], F.-P. Schilling[10], P. Schleper[10], S. Schmidt[27], S. Schmitt[39], M. Schneider[22], L. Schoeffel[9], A. Schöning[38], V. Schröder[10], H.-C. Schultz-Coulon[14], C. Schwanenberger[10], K. Sedlák[31], F. Sefkow[10], I. Sheviakov[26], L.N. Shtarkov[26], Y. Sirois[29], T. Sloan[17], P. Smirnov[26], Y. Soloviev[26], D. South[10], V. Spaskov[8], A. Specka[29], H. Spitzer[11], R. Stamen[10], B. Stella[33], J. Stiewe[14], I. Strauch[10], U. Straumann[39], G. Thompson[19], P.D. Thompson[3], F. Tomasz[14], D. Traynor[19], P. Truöl[39], G. Tsipolitis[10,40], I. Tsurin[37], J. Turnau[6], E. Tzamariudaki[27], A. Uraev[25], M. Urban[39], A. Usik[26], D. Utkin[25], S. Valkár[32], A. Valkárová[32], C. Vallée[22], P. Van Mechelen[4], A. Vargas Trevino[7], S. Vassiliev[8], Y. Vazdik[26], C. Veelken[18], A. Vest[1], A. Vichnevski[8], S. Vinokurova[10], V. Volchinski[36], K. Wacker[7], J. Wagner[10], G. Weber[11], R. Weber[38], D. Wegener[7], C. Werner[13], N. Werner[39], M. Wessels[1], B. Wessling[11], G.-G. Winter[10], Ch. Wissing[7], E.-E. Woehrling[3], R. Wolf[13], E. Wünsch[10], S. Xella[39], W. Yan[10], J. Žáček[32], J. Zálešák[32], Z. Zhang[28], A. Zhokin[25], H. Zohrabyan[36], F. Zomer[28]

[1] I. Physikalisches Institut der RWTH, Aachen, Germany[a]
[2] III. Physikalisches Institut der RWTH, Aachen, Germany[a]
[3] School of Physics and Space Research, University of Birmingham, Birmingham, UK[b]
[4] Inter-University Institute for High Energies ULB-VUB, Brussels; Universiteit Antwerpen (UIA), Antwerpen, Belgium[c]
[5] Rutherford Appleton Laboratory, Chilton, Didcot, UK[b]
[6] Institute for Nuclear Physics, Cracow, Poland[d]

[7] Institut für Physik, Universität Dortmund, Dortmund, Germany[a]
[8] Joint Institute for Nuclear Research, Dubna, Russia
[9] CEA, DSM/DAPNIA, CE-Saclay, Gif-sur-Yvette, France
[10] DESY, Hamburg, Germany
[11] Institut für Experimentalphysik, Universität Hamburg, Hamburg, Germany[a]
[12] Max-Planck-Institut für Kernphysik, Heidelberg, Germany
[13] Physikalisches Institut, Universität Heidelberg, Heidelberg, Germany[a]
[14] Kirchhoff-Institut für Physik, Universität Heidelberg, Heidelberg, Germany[a]
[15] Institut für experimentelle und Angewandte Physik, Universität Kiel, Kiel, Germany
[16] Institute of Experimental Physics, Slovak Academy of Sciences, Košice, Slovak Republic[e,f]
[17] Department of Physics, University of Lancaster, Lancaster, UK[b]
[18] Department of Physics, University of Liverpool, Liverpool, UK[b]
[19] Queen Mary and Westfield College, London, UK[b]
[20] Physics Department, University of Lund, Lund, Sweden[g]
[21] Physics Department, University of Manchester, Manchester, UK[b]
[22] CPPM, CNRS/IN2P3 – Univ Mediterranee, Marseille – France
[23] Departamento de Fisica Aplicada, CINVESTAV, Mérida, Yucatán, México[k]
[24] Departamento de Fisica, CINVESTAV, México[k]
[25] Institute for Theoretical and Experimental Physics, Moscow, Russia[l]
[26] Lebedev Physical Institute, Moscow, Russia[e]
[27] Max-Planck-Institut für Physik, München, Germany
[28] LAL, Université de Paris-Sud, IN2P3-CNRS, Orsay, France
[29] LLR, Ecole Polytechnique, IN2P3-CNRS, Palaiseau, France
[30] LPNHE, Universités Paris VI and VII, IN2P3-CNRS, Paris, France
[31] Institute of Physics, Academy of Sciences of the Czech Republic, Praha, Czech Republic[e,i]
[32] Faculty of Mathematics and Physics, Charles University, Praha, Czech Republic[e,i]
[33] Dipartimento di Fisica Università di Roma Tre and INFN Roma 3, Roma, Italy
[34] Paul Scherrer Institut, Villigen, Switzerland
[35] Fachbereich Physik, Bergische Universität Gesamthochschule Wuppertal, Wuppertal, Germany
[36] Yerevan Physics Institute, Yerevan, Armenia
[37] DESY, Zeuthen, Germany
[38] Institut für Teilchenphysik, ETH, Zürich, Switzerland[j]
[39] Physik-Institut der Universität Zürich, Zürich, Switzerland[j]
[40] Also at Physics Department, National Technical University, Zografou Campus, 15773 Athens, Greece
[41] Also at Rechenzentrum, Bergische Universität Gesamthochschule Wuppertal, Germany
[42] Also at Institut für Experimentelle Kernphysik, Universität Karlsruhe, Karlsruhe, Germany
[43] Also at University of P.J. Šafárik, Košice, Slovak Republic
[44] Also at CERN, Geneva, Switzerland
[†] Deceased

Received: 16 March 2004 / Revised version: 24 May 2004 /
Published online: 30 July 2004 – © Springer-Verlag / Società Italiana di Fisica 2004

Abstract. A search for squarks in R-parity violating supersymmetry is performed in $e^{\pm}p$ collisions at HERA using the H1 detector. The data were taken at a centre-of-mass energy of 319 GeV and correspond to an integrated luminosity of $64.3\,\mathrm{pb}^{-1}$ for $e^{+}p$ collisions and $13.5\,\mathrm{pb}^{-1}$ for $e^{-}p$ collisions. The resonant production of squarks via a Yukawa coupling λ' is considered, taking into account direct and indirect R-parity violating decay modes. No evidence for squark production is found in the multi-lepton and multi-jet final state topologies investigated. Mass dependent limits on λ' are obtained in the framework of the Minimal Supersymmetric Standard Model. In addition, the results are interpreted in terms of constraints on the parameters of the minimal Supergravity model. At the 95 % confidence level squarks of all flavours with masses up to 275 GeV are excluded in a large part of the parameter space for a Yukawa coupling of electromagnetic strength. For a coupling strength 100 times smaller, masses up to 220 GeV can be ruled out.

[a] Supported by the Bundesministerium für Bildung und Forschung, FRG, under contract numbers 05 H1 1GUA /1, 05 H1 1PAA /1, 05 H1 1PAB /9, 05 H1 1PEA /6, 05 H1 1VHA /7 and 05 H1 1VHB /5
[b] Supported by the UK Particle Physics and Astronomy Research Council, and formerly by the UK Science and Engineering Research Council
[c] Supported by FNRS-FWO-Vlaanderen, IISN-IIKW and IWT
[d] Partially Supported by the Polish State Committee for Scientific Research, SPUB/DESY/P003/DZ 118/2003/2005

1 Introduction

The ep collider HERA is ideally suited to search for new particles coupling to electron[1]–quark pairs. In supersymmetric models (SUSY) with R-parity violation ($\not{R}_p$), squarks can couple to electrons and quarks via Yukawa couplings λ'. At HERA, squarks could be produced resonantly via the fusion of the incoming 27.6 GeV electron and a quark from the incoming 920 GeV proton. Squark masses up to the electron-proton centre-of-mass energy, $\sqrt{s} = 319\,\text{GeV}$, are kinematically accessible.

This paper describes a search for squarks of all flavours using H1 data corresponding to an integrated luminosity of $64.3\,\text{pb}^{-1}$ for e^+p collisions and $13.5\,\text{pb}^{-1}$ for e^-p collisions. The search is carried out in the framework of the Minimal Supersymmetric Standard Model (MSSM) in the presence of a non-vanishing λ'. The analysis covers the major event topologies from direct and indirect $\not{R}_p$ squark decays such that the results can be interpreted in terms of a wide range of SUSY parameters. The search presented here supersedes the results previously obtained by H1 [1,2] at a lower centre-of-mass energy ($\sqrt{s} \approx 300\,\text{GeV}$) and with fewer data. Complementary searches for $\not{R}_p$ SUSY have been carried out at the LEP e^+e^- collider [3–5] and at the TeVatron $p\bar{p}$ collider [6,7].

2 Phenomenology

In the most general supersymmetric theory that is renormalisable and gauge invariant with respect to the Standard Model (SM) gauge group, the R-parity $R_p = (-1)^{3B+L+2S}$, where B denotes the baryon number, L the lepton number and S the spin of a particle, is not conserved. Couplings between two ordinary fermions and a squark ($\tilde{q}$) or a slepton ($\tilde{l}$) are then allowed. The $\not{R}_p$ Yukawa couplings responsible for squark production at HERA are described in the superpotential by the terms $\lambda'_{ijk} L_i Q_j \overline{D}_k$, where i, j and k are family indices. L_i, Q_j and D_k are superfields, which contain the left-handed leptons, the left-handed quarks and the right-handed down quark, respectively, together with their SUSY partners $\tilde{l}^i_L$, $\tilde{q}^j_L$ and $\tilde{d}^k_R$. The corresponding part of the Lagrangian expanded in fields is given by

$$\mathcal{L}_{L_i Q_j \overline{D}_k} = \lambda'_{ijk} \Big[-\tilde{e}^i_L u^j_L \bar{d}^k_R - e^i_L \tilde{u}^j_L \bar{d}^k_R - (\bar{e}^i_L)^c u^j_L \tilde{d}^{k*}_R + \tilde{\nu}^i_L d^j_L \bar{d}^k_R + \nu_L \tilde{d}^j_L \bar{d}^k_R + (\bar{\nu}^i_L)^c d^j_L \tilde{d}^{k*}_R \Big] + \text{c.c.}, \quad (1)$$

where the superscript c denotes the charge conjugate of a spinor and $*$ the complex conjugate of a scalar field. Non-vanishing couplings λ'_{1jk} allow the resonant production of squarks at HERA through eq fusion [8]. The values of the couplings are not fixed by the theory. For simplicity, it is assumed here that one of the λ'_{1jk} dominates over all other possible trilinear couplings.

For the nine possible couplings λ'_{1jk}, the corresponding squark production processes in $e^\pm p$ reactions are listed in Table 1. At high Bjorken-x the density of antiquarks in the proton is smaller than that of quarks. Thus e^-p scattering gives the best sensitivity to the couplings λ'_{11k} ($k = 1,2,3$), where mainly $\tilde{d}_R$-type squarks (*i.e.* the superpartners $\tilde{d}_R, \tilde{s}_R$ and $\tilde{b}_R$ of right-handed quarks) can be produced. The dominant squark production cross section in e^-p collisions is approximately proportional to $\lambda'^2_{11k} \cdot u(x)$ where $u(x)$ is the probability of finding a u quark in the proton with a momentum fraction $x = M^2_{\tilde{q}}/s$, $M_{\tilde{q}}$ being the squark mass. In contrast, e^+p scattering gives the best sensitivity to the couplings λ'_{1j1} ($j = 1,2,3$), where mainly $\tilde{u}_L$-type squarks (*i.e.* the superpartners $\tilde{u}_L, \tilde{c}_L$ and $\tilde{t}_L$ of left-handed quarks) can be produced. Here the dominant squark production cross section is approximately proportional to $\lambda'^2_{1j1} \cdot d(x)$. Since the u quark density in the proton is larger than the d quark density at large x, the squark production cross section in e^-p interactions is larger than that in the e^+p case for comparable couplings and squark masses.

In this work the signal cross section is obtained in the narrow width approximation from the leading order (LO) amplitudes given in [9], corrected by multiplicative factors [10] to account for next-to-leading order QCD corrections. The parton densities are evaluated at the hard scale $M^2_{\tilde{q}}$. For cases, where the squark width is not negligible, the approach given in [11] is followed.

In $\not{R}_p$ SUSY all supersymmetric particles are unstable. Squarks can decay via their Yukawa coupling λ' into SM fermions. According to equation (1), the $\tilde{d}_R$-type squarks can decay either into $e^- + u^j$ or $\nu_e + d^j$, while the $\tilde{u}_L$-type squarks decay into $e^+ + d^k$ only. The $\not{R}_p$ squark decays, proceeding directly via the couplings λ'_{11k} and λ'_{1j1}, are illustrated in Fig. 1.

Squarks can also decay via their usual R_p conserving gauge couplings, as shown in Fig. 2. The $\tilde{u}_L$-type squarks can undergo a gauge decay into states[2] involving a neutralino χ^0_i ($i = 1 \ldots 4$), a chargino χ^+_i ($i = 1,2$) or a gluino $\tilde{g}$. In contrast, $\tilde{d}_R$-type squarks decay to χ^0_i or $\tilde{g}$ only and decays into charginos are suppressed, since the supersymmetric partners of right-handed quarks do not couple to winos.

The final state of these gauge decays depends on the subsequent gaugino decay, of which examples are shown

[e] Supported by the Deutsche Forschungsgemeinschaft
[f] Supported by VEGA SR grant no. 2/1169/2001
[g] Supported by the Swedish Natural Science Research Council
[i] Supported by the Ministry of Education of the Czech Republic under the projects INGO-LA116/2000 and LN00A006, by GAUK grant no 173/2000
[j] Supported by the Swiss National Science Foundation
[k] Supported by CONACYT, México, grant 400073-F
[l] Partially Supported by Russian Foundation for Basic Research, grant no. 00-15-96584

[1] In the following the term *electron* will be used to refer to both electron and positron unless explicitly stated otherwise.

[2] The mass eigenstates χ^0_i ($\chi^\pm_i$) are mixed states of the photino, the zino and the neutral higgsinos (the winos and the charged higgsinos). The $\tilde{g}$ is the SUSY partner of the gluon.

Table 1. Squark production processes in $e^{\pm}p$ collisions for different Yukawa couplings λ'_{1jk}. The $\tilde{q}_R$ and $\tilde{q}_L$ symbols denote the squarks which are superpartners of the right- and left-handed quarks, respectively. Their antimatter counterparts are denoted by $\bar{\tilde{q}}_R$ and $\bar{\tilde{q}}_L$

λ'_{1jk}	e^-p		e^+p	
111	$e^- + u \to \tilde{d}_R$	$e^- + \overline{d} \to \bar{\tilde{u}}_L$	$e^+ + d \to \tilde{u}_L$	$e^+ + \overline{u} \to \bar{\tilde{d}}_R$
112	$e^- + u \to \tilde{s}_R$	$e^- + \overline{s} \to \bar{\tilde{u}}_L$	$e^+ + s \to \tilde{u}_L$	$e^+ + \overline{u} \to \bar{\tilde{s}}_R$
113	$e^- + u \to \tilde{b}_R$	$e^- + \overline{b} \to \bar{\tilde{u}}_L$	$e^+ + b \to \tilde{u}_L$	$e^+ + \overline{u} \to \bar{\tilde{b}}_R$
121	$e^- + c \to \tilde{d}_R$	$e^- + \overline{d} \to \bar{\tilde{c}}_L$	$e^+ + d \to \tilde{c}_L$	$e^+ + \overline{c} \to \bar{\tilde{d}}_R$
122	$e^- + c \to \tilde{s}_R$	$e^- + \overline{s} \to \bar{\tilde{c}}_L$	$e^+ + s \to \tilde{c}_L$	$e^+ + \overline{c} \to \bar{\tilde{s}}_R$
123	$e^- + c \to \tilde{b}_R$	$e^- + \overline{b} \to \bar{\tilde{c}}_L$	$e^+ + b \to \tilde{c}_L$	$e^+ + \overline{c} \to \bar{\tilde{b}}_R$
131	$e^- + t \to \tilde{d}_R$	$e^- + \overline{d} \to \bar{\tilde{t}}_L$	$e^+ + d \to \tilde{t}_L$	$e^+ + \overline{t} \to \bar{\tilde{d}}_R$
132	$e^- + t \to \tilde{s}_R$	$e^- + \overline{s} \to \bar{\tilde{t}}_L$	$e^+ + s \to \tilde{t}_L$	$e^+ + \overline{t} \to \bar{\tilde{s}}_R$
133	$e^- + t \to \tilde{b}_R$	$e^- + \overline{b} \to \bar{\tilde{t}}_L$	$e^+ + b \to \tilde{t}_L$	$e^+ + \overline{t} \to \bar{\tilde{b}}_R$

in Fig. 2. Neutralinos χ^0_i with $i > 1$ as well as charginos (gluinos) are expected to undergo gauge decays into a lighter χ and two SM fermions (two quarks), through a real or virtual gauge boson or sfermion (squark). The decay chain ends with the $\not{R}_p$ decay of one sparticle, usually the lightest supersymmetric particle (LSP), assumed here to be a χ^0, $\chi^{\pm}$ or $\tilde{g}$. $\not{R}_p$ decays of gauginos are mainly relevant for the lightest states. Neutralinos may undergo the $\not{R}_p$ decays $\chi^0 \to e^{\pm} q \bar{q}'$ or $\chi^0 \to \nu q \bar{q}$, the former (latter) being more frequent if the χ^0 is dominated by its photino (zino) component. Gluinos can undergo the same $\not{R}_p$ decays. When a χ^0 or a $\tilde{g}$ decays via an $\not{R}_p$ coupling into a charged lepton, both the "right" and the "wrong" charge lepton (with respect to the incident beam) are equally probable, the latter case leading to striking, largely background-free signatures for lepton number violation. In contrast, the only possible $\not{R}_p$ decays for charginos are $\chi^+ \to \bar{\nu} u^k \bar{d}^j$ and $\chi^+ \to e^+ d^k \bar{d}^j$.

The $\tilde{u}^j_L$ ($\tilde{d}^k_R$) decay chains analysed in this paper are classified by event topology, as described in Table 2. This classification relies on the number of charged leptons and/or hadronic jets in the final state, and on the presence of missing momentum. The channels labelled eq and νq are the squark decay modes which proceed directly via $\not{R}_p$ couplings, while the remaining channels result from the gauge decays of the squark and are characterised by multijet (MJ) final states. The channels labelled e^+MJ, e^-MJ and νMJ involve one or two SUSY fermions (χ or $\tilde{g}$) denoted by X and Y in Table 2. The channels $e\ell MJ$ and $\nu\ell MJ$ necessarily involve two SUSY fermions.

Decay patterns involving more than two gauginos are kinematically suppressed and are therefore not explicitly studied here. Processes leading to final states with tau leptons are also not explicitly investigated. Cases where the

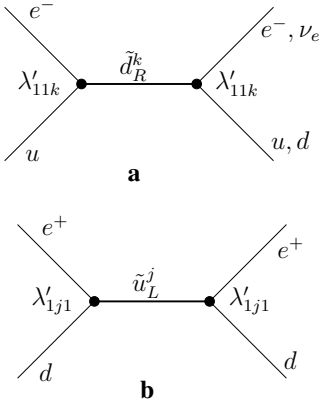

Fig. 1. Lowest order s-channel diagrams for $\not{R}_p$ squark production via the Yukawa coupling λ' in (a) e^-p and (b) e^+p interactions, followed by $\not{R}_p$ squark decays

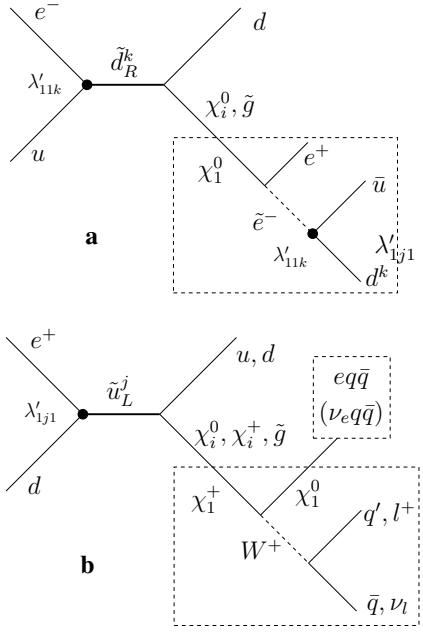

Fig. 2. Gauge decays of squarks. Example decays of the emerging neutralino, chargino or gluino are shown in the dashed boxes for (a) the χ^0_1 and (b) the χ^+_1

Table 2. Squark decay channels in $\not{R}_p$ SUSY classified by event topology. X and Y denote a neutralino, a chargino or a gluino. The $\not{R}_p$ process is indicated by λ'

Channel	Decay process						Event topology
eq	$\tilde{q}$	$\xrightarrow{\lambda'}$	e	q			high p_T e + 1 jet
νq	$\tilde{d}^k_R$	$\xrightarrow{\lambda'}$	ν_e	d			missing p_T + 1 jet
$e^{\pm}MJ$	$\tilde{q}$	$\longrightarrow$	q	X			e (both charges) + multiple jets
				$\overset{\lambda'}{\hookrightarrow}$	$e^{\pm}\bar{q}q$		
	$\tilde{q}$	$\longrightarrow$	q	X			
				$\hookrightarrow$	$q\bar{q}$	Y	
						$\overset{\lambda'}{\hookrightarrow} e^{\pm}\bar{q}q$	
νMJ	$\tilde{q}$	$\longrightarrow$	q	X			missing p_T + multiple jets
				$\overset{\lambda'}{\hookrightarrow}$	$\nu\bar{q}q$		
	$\tilde{q}$	$\longrightarrow$	q	X			
				$\hookrightarrow$	$q\bar{q}$	Y	
						$\overset{\lambda'}{\hookrightarrow} \nu\bar{q}q$	
	$\tilde{q}$	$\longrightarrow$	q	X			
				$\hookrightarrow$	$\nu\bar{\nu}$	Y	
						$\overset{\lambda'}{\hookrightarrow} \nu\bar{q}q$	
$elMJ$	$\tilde{q}$	$\longrightarrow$	q	X			e + ℓ (e or μ) + multiple jets
				$\hookrightarrow$	$\ell\nu_\ell$	Y	
						$\overset{\lambda'}{\hookrightarrow} e^{\pm}\bar{q}q$	
	$\tilde{q}$	$\longrightarrow$	q	X			
				$\hookrightarrow$	$\ell^+\ell^-$	Y	
						$\overset{\lambda'}{\hookrightarrow} e^{\pm}\bar{q}q$	
	$\tilde{q}$	$\longrightarrow$	q	X			
				$\hookrightarrow$	e^+e^-	Y	
						$\overset{\lambda'}{\hookrightarrow} \nu\bar{q}q$	
νlMJ	$\tilde{q}$	$\longrightarrow$	q	X			ℓ (e or μ) + missing p_T + multiple jets
				$\hookrightarrow$	$\ell\nu_\ell$	Y	
						$\overset{\lambda'}{\hookrightarrow} \nu\bar{q}q$	
	$\tilde{q}$	$\longrightarrow$	q	X			
				$\hookrightarrow$	$\nu\bar{\nu}$	Y	
						$\overset{\lambda'}{\hookrightarrow} e\bar{q}q$	
	$\tilde{q}$	$\longrightarrow$	q	X			
				$\hookrightarrow$	$\mu^+\mu^-$	Y	
						$\overset{\lambda'}{\hookrightarrow} \nu\bar{q}q$	

χ^0_1 has such a long lifetime that large displaced vertices are expected are not considered, since the region of parameter space that allows a χ^0_1 to escape detection for a finite value of the $\not{R}_p$ coupling is very strongly constrained by the searches for gauginos carried out at LEP [5]. Decays of a χ into states involving a Higgs boson are taken into account when the Higgs decays into hadrons. The contribution of these decays is, however, very small.

3 The H1 detector

A detailed description of the H1 experiment can be found in [12]. The main components of the tracking system are the central drift and proportional chambers which cover the polar angle[3] range $25° \leq \theta \leq 155°$, a forward track detector ($7° \leq \theta \leq 25°$) and a backward drift chamber.

[3] The polar angle θ is measured with respect to the direction of the outgoing proton beam ($+z$).

The tracking system is surrounded by a finely segmented liquid argon (LAr) calorimeter [13] which covers the polar angle range $4^\circ \leq \theta \leq 154^\circ$ and has an energy resolution of $\sigma(E)/E \simeq 12\%/\sqrt{E/\mathrm{GeV}} \oplus 1\%$ for electrons and $\sigma(E)/E \simeq 50\%/\sqrt{E/\mathrm{GeV}} \oplus 2\%$ for hadrons, as obtained in test beam measurements [14]. The tracking chambers and the LAr are surrounded by a superconducting solenoid and its iron yoke instrumented with streamer tubes. The latter are used to detect hadronic showers which extend beyond the LAr and to identify muons. The luminosity is determined from the rate of Bethe-Heitler events ($ep \to ep\gamma$) measured in a luminosity monitor.

4 Monte Carlo event generation

In order to estimate the amount of SM background in the various squark decay channels and to determine the signal detection efficiencies, complete simulations of the H1 detector response are performed for various Monte Carlo (MC) samples.

For each possible SM background source, a sample of MC events is used, corresponding to a luminosity of more than ten times that of the data. The determination of the contribution of neutral current (NC) deep inelastic scattering (DIS) processes is performed using two MC programs which both include LO QCD matrix elements but employ different models of QCD radiation. The first is produced with the DJANGO [15] event generator, where QCD radiation is implemented using ARIADNE [16], based on the Colour Dipole Model (CDM) [17]. This sample is chosen to estimate the NC DIS contribution in the eq channel. The second sample is generated with the program RAPGAP [18], where higher order QCD radiation is modelled using leading-log DGLAP parton showers [19]. This sample is used to determine the NC DIS background in the final states with an electron and multiple jets, as RAPGAP gives the better description of this particular phase space domain [11]. For both samples, the parton densities in the proton are taken from the CTEQ5L [20] parameterisation. Hadronisation is performed in the Lund string fragmentation scheme using JETSET [21]. The modelling of the charged current (CC) DIS process is performed using the DJANGO program with CTEQ5L parton densities. The direct and resolved photoproduction (γp) of light and heavy flavours, including prompt photon production, is generated using the PYTHIA [22] program, which relies on first order matrix elements and uses leading-log parton showers and string fragmentation. The SM expectations for $ep \to eW^{\pm}X$ and $ep \to eZ^0X$ are calculated using EPVEC [23]. The LO MC simulations used to model QCD multi-jet production give only approximate descriptions of the kinematic distributions. From a comparison of various kinematic distributions between the data and the LO MC simulations for a loose multi-jet preselection, a normalisation factor of 1.2 is derived [11], which is applied to the yield of multi-jet events predicted by RAPGAP and PYTHIA.

To allow a model independent interpretation of the results, the squark decay processes given in Table 2 are simulated separately for a wide range of masses of the SUSY particles involved. The LEGO [24] event generator is used for the determination of the signal detection efficiencies in the eq and νq channels, whereas for the gauge decays of squarks the SUSYGEN [25] generator is used. The squark mass is varied from 100 GeV to 290 GeV in steps of typically 25 GeV. For all gauge decays of squarks involving one gaugino which decays directly via $\not{R}_p$ (*i.e.* processes corresponding to the first line of the $e^{\pm}MJ$ and νMJ rows in Table 2), the process $\tilde{q} \to q\chi_1^0$ is simulated for χ_1^0 masses ranging between 30 GeV and $M_{\tilde{q}}$. In order to study all cascade gauge decays which involve two gauginos, the processes $\tilde{q} \to q\chi_1^+ \to q\chi_1^0 f\bar{f}'$ and $\tilde{q} \to q\chi_2^0 \to q\chi_1^0 f\bar{f}'$ are simulated for χ_1^+ and χ_2^0 masses ranging between 40 GeV and $M_{\tilde{q}}$, and for χ_1^0 masses between 30 GeV and $M_{\chi_1^+}$ or $M_{\chi_2^0}$. The masses of the χ's are varied in steps of typically 10 GeV. The lower mass values for squarks and χ's are motivated by the exclusion domains resulting from $\not{R}_p$ SUSY searches considering non-vanishing couplings λ' at LEP [4, 5]. The simulations allow the determination of signal detection efficiencies as a function of the masses of the SUSY particles involved, since the mass intervals are sufficiently small for linear interpolations to be used.

5 Searches for SUSY signals

5.1 Basic event selection

The recording of the events used in this analysis is triggered using the LAr system [13], with an efficiency close to 100 %. Background events not related to ep collisions are suppressed by requiring that a primary interaction vertex be reconstructed within ± 35 cm in z of the nominal vertex position and by using topological filters against cosmic and proton-beam related background. The event time as determined by the central drift chambers is required to be consistent with the bunch crossing time.

5.2 Particle identification and kinematic reconstruction

The following criteria are used to select events containing leptons, high transverse momentum jets or missing transverse energy. An **electron** is identified as an isolated and compact electromagnetic cluster of energy greater than 11 GeV in the LAr. For electrons in the central detector region ($30^\circ < \theta_e < 145^\circ$) a charged track pointing to the electromagnetic cluster is required. A **muon** candidate is identified as a track measured in the central or forward tracking system, which matches geometrically with a track in the instrumented iron, a track in the forward muon detector or an energy deposit in the LAr calorimeter compatible with that expected from a minimum ionising particle. **Hadronic jets** are reconstructed from energy deposits in the calorimeter using a cone algorithm in the laboratory frame with a radius $\sqrt{\Delta\eta^2 + \Delta\phi^2} = 1$, where $\eta = -\ln\tan\frac{\theta}{2}$ is the pseudorapidity and ϕ denotes the azimuthal angle. The **missing transverse momentum**

$p_{T,\mathrm{miss}}$ is obtained by the summation of all the energy deposits in the calorimeter.

For further selection the following Lorentz invariants are important:

$$y_e = 1 - \frac{E_e(1-\cos\theta_e)}{2E_e^0}; \qquad Q_e^2 = \frac{p_{T,e}^2}{1-y_e};$$
$$x_e = \frac{Q_e^2}{y_e s}; \qquad M_e = \sqrt{x_e s}\ .$$

They are determined using the measurement of the polar angle θ_e, the energy E_e and the transverse momentum $p_{T,e}$ of the electron with the highest p_T found in the event. E_e^0 denotes the energy of the incident electron. Similar quantities can be calculated using the Jacquet-Blondel method [26]:

$$y_h = \frac{\sum (E-p_z)_h}{2E_e^0}; \qquad Q_h^2 = \frac{p_{T,h}^2}{1-y_h};$$
$$x_h = \frac{Q_h^2}{y_h s}; \qquad M_h = \sqrt{x_h s}\ ;$$

where $p_{T,h}$ and $\sum(E-p_z)_h$ are calculated from the hadronic energy deposits in the calorimeter.

5.3 Systematic uncertainties

In each selection channel the systematic errors on the SM background expectation are evaluated by considering the following uncertainties.

- The uncertainty on the electromagnetic energy scale of the calorimeter varies from 0.7 % to 3 % depending on the calorimeter region [27].
- The uncertainty on the hadronic energy scale is 2 %.
- The uncertainty on the integrated luminosity is 1.5 %.
- An uncertainty of ±7 % on the DIS expectation arises from the parton densities of the proton at high x.
- An uncertainty of ±10 % on the predicted cross section for multi-jet final states is estimated by comparing the LO MC simulations where higher order QCD radiation is modelled by either the CDM or DGLAP parton showers.

Furthermore, the following uncertainties related to the modelling of the SUSY signal are taken into account.

- The theoretical uncertainty on the signal cross sections due to uncertainties in the parton densities varies from 7 % for $e^- u \to \tilde{d}_R^k$ at low squark masses up to 50 % for $e^+ d \to \tilde{u}_L^j$ at high masses.
- Choosing either Q^2 or the square of the transverse momentum of the final state lepton in squark decays (proceeding directly via the coupling λ') instead of $M_{\tilde{q}}^2$ as the hard scale at which the parton distributions are determined yields an uncertainty of ±7 % on the signal cross section.
- An uncertainty of 10 % is attributed to the signal detection efficiencies, resulting mainly from the interpolation between the simulated mass values.

5.4 R-parity violating squark decays

5.4.1 Selection channel eq

The final state with an electron and a jet of high transverse momentum, resulting from squarks decaying in the channel eq, corresponds exactly to the NC DIS signature at high x. However, the M_e and y_e distributions of the two processes differ. Squark decays via $\not{R}_p$ lead to a resonance in the M_e distribution which is measured with a resolution of between 3 and 6 GeV depending on the squark mass. Squarks produced in the s-channel decay isotropically in their rest frame, leading to a flat $d\sigma/dy$ distribution. In contrast, the distribution for NC DIS varies approximately as $d\sigma/dy \propto y^{-2}$.

The selection criteria for the eq channel are the following.

- The total transverse momentum of the events must be balanced: $p_{T,\mathrm{miss}} < 15$ GeV.
- The reconstructed momentum loss in the direction of the momentum of the incoming electron must be such that $40 \le \sum(E-p_z) \le 70$ GeV, where the sum extends over all reconstructed particles.
- An electron must be found in the LAr calorimeter with $p_{T,e} > 16$ GeV.
- To improve the sensitivity, the differences in the M_e and y_e distributions of the SUSY signal and the DIS background are exploited by applying a lower y_e-cut which depends on the mass of the squark under consideration. The y_e-cut is optimised by minimising the expected limit. It ranges from 0.5 for masses around 100 GeV to 0.2 around 290 GeV [11].
- The selection is restricted to the kinematic range $Q_e^2 > 2500\,\mathrm{GeV}^2$ and $y_e < 0.9$. Excluding the highest y_e values avoids the region where migration effects due to initial state QED radiation are largest. Furthermore, background from photoproduction events, in which hadrons are misidentified as electrons, is suppressed.
- To ensure that the various selections are exclusive[4], all events accepted in one of the selection channels with an electron and several jets (Sect. 5.5) are not accepted in the eq channel. About 10 % of the candidate events are removed from the eq channel by this requirement.

The M_e spectra for the data and the SM background simulation after this selection are shown in Fig. 3 for e^+p and e^-p collisions. No significant deviation from the SM expectation is found for either data sample. Table 3 gives the total numbers of selected events and the SM expectation. In the e^+p data set 632 candidate events are found, which is to be compared with 628 ± 46 expected from SM processes. In the e^-p data sample, 204 events are observed while the SM expectation is 192 ± 14.

5.4.2 Selection channel νq

Squarks undergoing a direct $\not{R}_p$ decay into νq lead to CC DIS-like events with high missing transverse momentum.

[4] This is necessary for the limit calculations (Sect. 6).

Table 3. Total numbers of selected events, SM expectations and ranges of selection efficiencies of the squark decay channels considered in e^+p and in e^-p collisions. The $\tilde{u}_L$-type squarks (e^+p collisions) cannot decay to νq

	e^+p collisions		e^-p collisions		
Channel	Data	SM expectation	Data	SM expectation	Efficiency
eq	632	628 ± 46	204	192 ± 14	$30-50\,\%$
νq	—	—	261	269 ± 21	$40-60\,\%$
eMJ ("right" charge)	72	67.5 ± 9.5	20	17.9 ± 2.4	$15-50\,\%$
eMJ ("wrong" charge)	0	0.20 ± 0.14	0	0.06 ± 0.02	$10-30\,\%$
$eeMJ$	0	0.91 ± 0.51	0	0.13 ± 0.03	$15-45\,\%$
$e\mu MJ$	0	0.91 ± 0.38	0	0.20 ± 0.04	$15-35\,\%$
νeMJ	0	0.74 ± 0.26	0	0.21 ± 0.07	$15-40\,\%$
νMJ	30	24.3 ± 3.6	12	10.1 ± 1.4	$10-60\,\%$
$\nu\mu MJ$	0	0.61 ± 0.12	0	0.16 ± 0.03	$15-50\,\%$

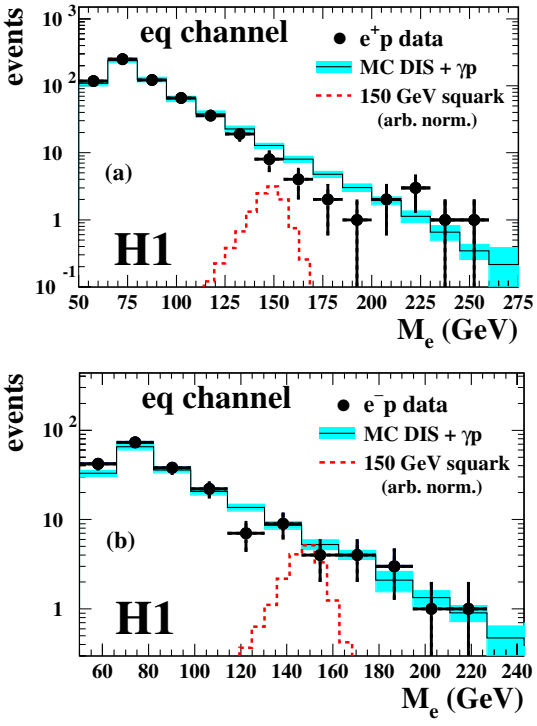

Fig. 3. Mass spectra for the eq selection channel in **a** e^+p and **b** e^-p collisions. The shaded error band indicates the uncertainty on the SM background. The signal expected for a squark of mass 150 GeV is shown with arbitrary normalisation (dashed histogram). Events with an electron and multiple jets are not included in the spectra

The events are expected to cluster in the M_h distribution with a resolution of 10 to 20 GeV, depending on the squark mass.

The selection criteria for the νq channel are the following:

- The missing transverse momentum must be greater than 30 GeV.
- No electron or muon must be found with $p_T > 5$ GeV.

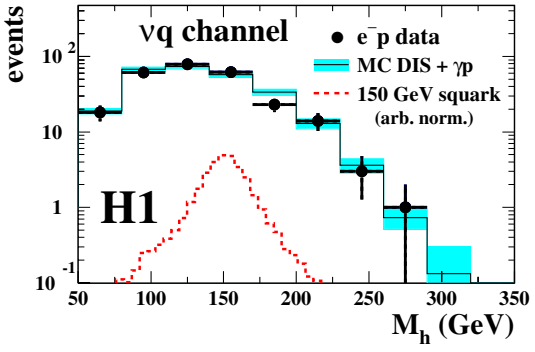

Fig. 4. Mass spectrum for the νq selection channel in e^-p collisions. The shaded error band indicates the uncertainty on the SM background. The signal expected for a squark of mass 150 GeV is shown with arbitrary normalisation (dashed histogram). Events accepted in the selection channel νMJ are not included in the spectra

- The events must lie in the kinematic range $Q_h^2 > 2500\,\mathrm{GeV}^2$ and $y_h < 0.9$. The resolutions in both M_h and Q_h^2 degrades with increasing y_h since both $\delta M_h/M_h$ and $\delta Q_h^2/Q_h^2$ behave as $1/(1-y_h)$ for $y_h \sim 1$. Hence the high y_h range is excluded.
- To ensure exclusivity with respect to the νMJ channel (Sect. 5.6), events with two or more jets with $p_{T,\mathrm{jet}} > 15$ GeV are rejected. This removes about 3.5 % of the candidate events.

Only $\tilde{d}_R$-type squarks, which are produced mainly in e^-p collisions, can undergo a decay into the νq final state. The M_h spectrum of this data set and the SM background are shown in Fig. 4. No significant deviation from the SM expectation is found. 261 events are observed in the data and 269 ± 21 are expected according to the SM.

5.5 Squark gauge decays leading to e + jets + X final states

For the channels e^+MJ, e^-MJ, $eeMJ$, $e\mu MJ$ and νeMJ a common preselection is carried out:

– At least one electron must be found with $p_{T,e} > 6\,\text{GeV}$ in the angular range $5° < \theta_e < 110°$. For central electrons ($\theta_e > 30°$) the charged track, measured in the central tracking system, must geometrically and kinematically match the electromagnetic cluster. To discriminate against fake-electron background from photoproduction, electron candidates in the forward region ($\theta_e < 30°$) have to fulfill harsher isolation criteria and the $\sum(E - p_z)$ of the event must be greater than 30 GeV. The latter cut causes only a small efficiency loss for all channels discussed here.
– At least two jets must be found with $p_{T,\text{jet}} > 15\,\text{GeV}$ in the range $7° < \theta_{\text{jet}} < 145°$.
– For all final state topologies considered here, the squark decay products are mainly emitted in the forward direction. This is exploited by requiring that:
  – $Q_e^2 > 1000\,\text{GeV}^2$.
  – At least one of the polar angles of the highest p_T electron and the two highest p_T jets is less than 40°.
  – Of the two jets with highest p_T, that with the larger polar angle θ_{backw} satisfies $\theta_{\text{backw}} < 180° \cdot (y_e - 0.3)$. This cut efficiently separates the SUSY signal events from the NC DIS background [11].

After this preselection, 91 (22) events are found in the e^+p (e^-p) data sample while 89.3 ± 3.7 (22.6 ± 0.7) is the SM expectation. Further cuts are applied for each sub-channel.

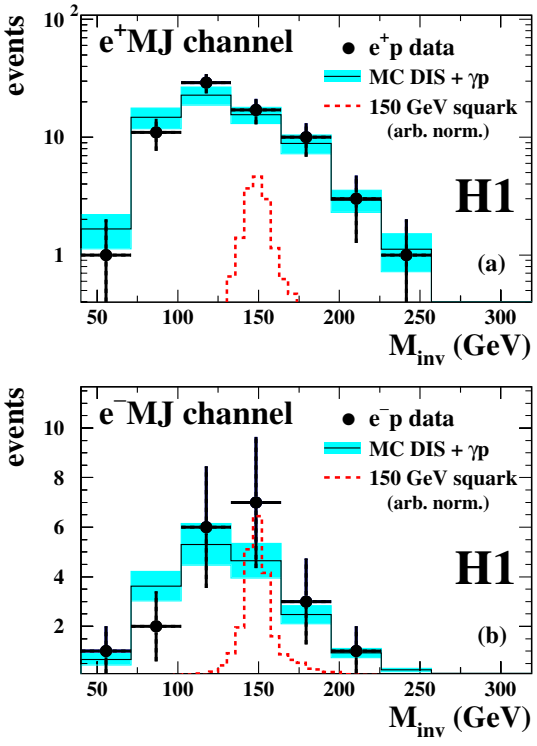

Fig. 5. Mass spectra for **a** the e^+MJ selection channel in e^+p collisions and **b** the e^-MJ selection channel in e^-p collisions. The shaded error band indicates the uncertainty on the SM background. The signal expected for a squark of mass 150 GeV is shown with arbitrary normalisation (dashed histogram)

5.5.1 Channels with "wrong" and "right" lepton charge

For the channels e^+MJ and e^-MJ no neutrinos are involved in the final state. Therefore the missing momentum is restricted according to $p_{T,\text{miss}} < 15\,\text{GeV}$ and $40 < \sum(E - p_z) < 70\,\text{GeV}$. To ensure that the selection is exclusive with respect to the $eeMJ$ and $e\mu MJ$ channels, events with a second electron with $p_{T,e} > 5\,\text{GeV}$ and $5° < \theta_e < 110°$, or a muon with $p_{T,\mu} > 5\,\text{GeV}$ and $10° < \theta_\mu < 110°$, are rejected.

Events are accepted in the channel having the "wrong" charge lepton, *i.e.* different from the incident beam, if the electron/positron is found in the angular range $\theta_e > 30°$ (where the charge measurement is made with the central tracking system) and the charge is measured to be opposite to that of the incident lepton, with a significance greater than two standard deviations. No candidates are found in the data and the SM expectation in this channel is very low (see Table 3).

In the "right" charge lepton channel, *i.e.* the same charge as the lepton beam, events are accepted if they contain either a central electron ($\theta_e > 30°$) with a charge measurement of the "right" sign or an electron found in the forward region ($\theta_e < 30°$). In the latter case no charge requirement is made. For the selected events, an invariant squark mass M_{inv} is calculated as: $M_{\text{inv}} = \sqrt{4E_e^0\,(\sum_i E_i - E_e^0)}$, where the sum runs over the electrons and the jets found in the event with $p_T > 5\,\text{GeV}$. This method yields a good reconstruction of the squark mass with a typical resolution of 7 to 10 GeV. The M_{inv} distributions for the data and the SM expectation are shown for the "right" charge eMJ channel in Fig. 5 for e^+p and e^-p collisions. No significant deviation from the SM is observed at any mass value. In total 72 (20) events are selected in the e^+p (e^-p) data set with 67.5 ± 9.5 (17.9 ± 2.4) predicted from SM background processes.

5.5.2 Channels with an additional lepton

The further selection for the channels $eeMJ$ and $e\mu MJ$ requires either an additional electron with the same criteria as described in the common preselection, or an additional muon with $p_{T,\mu} > 5\,\text{GeV}$ in the polar angle range $10° < \theta_\mu < 110°$. To ensure exclusivity, events are accepted in one selection channel ($eeMJ$ or $e\mu MJ$) only[5]. In these channels the SM background (mainly NC DIS) is very low (see Table 3). No candidate events for either $eeMJ$ or $e\mu MJ$ are found in either data set, which is compatible with the SM expectation.

For the channel νeMJ, candidate events, possibly containing a neutrino, are selected by requiring $p_{T,\text{miss}} > 15\,\text{GeV}$. A cut of $y_e(y_e - y_h) > 0.04$ exploits the fact that

[5] Events with a muon with $p_{T,\mu} > 5\,\text{GeV}$ and $10° < \theta_\mu < 110°$ are not accepted in the $eeMJ$ channel. Similarly, events with an additional electron in the range $5° < \theta_e < 110°$ are not accepted in the $e\mu MJ$ channel.

for the SUSY signal the escaping neutrino carries a non-negligible part of $\sum (E - p_z)$ and hence the variable y_h is substantially smaller than y_e, while $y_e \sim y_h$ is expected for NC DIS events. Events previously accepted in the $eeMJ$ or $e\mu MJ$ channels are rejected. No events are found in this channel. This is compatible with the SM expectation (mainly NC DIS) as detailed in Table 3.

5.6 Squark gauge decays leading to ν + jets + X final states

The selection of νMJ and $\nu\mu MJ$ candidates starts with the requirement that:

- The missing transverse momentum satisfies $p_{T,\mathrm{miss}} > 26\,\mathrm{GeV}$.
- At least two jets with $p_{T,\mathrm{jet}} > 15\,\mathrm{GeV}$ are reconstructed in the angular range $7^\circ < \theta_{\mathrm{jet}} < 145^\circ$.
- No electron is found in the event.

If no muon is found, the event is identified as a νMJ candidate. Assuming that the missing energy of a candidate event is carried by one neutrino only, its kinematics are reconstructed by exploiting energy-momentum conservation. The four-vector of this ν is then added to that of the hadronic final state to reconstruct the invariant mass M_{rec} of the incoming electron and quark. The mass resolution of this method is about 15 GeV. The M_{rec} spectra of the data and the expected SM background are shown in Fig. 6. In the e^+p (e^-p) data set 30 (12) νMJ candidate events are selected while 24.3 ± 3.6 (10.1 ± 1.4) are expected from SM background (mainly CC DIS).

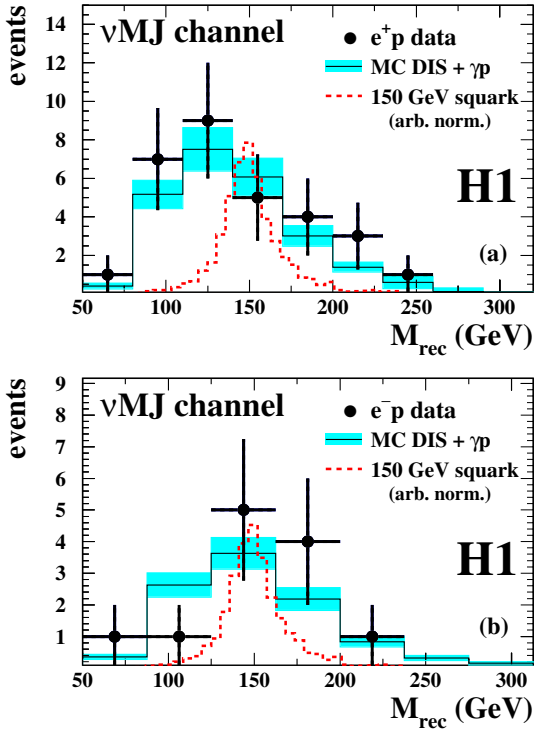

Fig. 6. Mass spectra for the νMJ selection channel in **a** e^+p and **b** e^-p collisions. The shaded error band indicates the uncertainty on the SM background. The signal expected for a squark of mass 150 GeV is shown with arbitrary normalisation (dashed histogram)

If in addition to the above requirements a muon with $p_{T,\mu} > 5\,\mathrm{GeV}$ in the range $10^\circ < \theta_\mu < 110^\circ$ is found, the events are identified as $\nu\mu MJ$ candidates. No candidate events are found in either data set. This is compatible with the SM expectation (predominantly CC DIS), which is shown in Table 3.

6 Exclusion limits

The total numbers of selected and expected events are summarised in Table 3 for all final state topologies considered in this analysis. It is assured by the choice of the selection cuts for the different channels that the selection of all topologies is fully exclusive. No significant deviation from the SM expectation is found in any channel. The selection channels are combined, separately for the e^+p and e^-p data sets, to derive constraints on $R\!\!\!/_p$ SUSY models.

6.1 Method of limit derivation

For a given set of parameters in a certain supersymmetric model, the full supersymmetric mass spectrum and the branching ratios of all squark decay modes are calculated using the SUSYGEN package. An upper limit N_{lim} on the number of events coming from squark production is calculated at a confidence level (CL) of 95 % using a modified frequentist approach based on Likelihood Ratios [28]. The following quantities enter the limit calculation.

- The numbers of events observed in the data for all selection channels. For the channels where the SM background is considerable (eq, νq, eMJ with "right" lepton charge and νMJ) the event numbers are integrated within a mass bin around the squark mass under consideration. For each decay channel the width of the mass bin is optimised, *i.e.* the expected limit is minimised, using the reconstructed mass distributions from the SUSY signal and SM background simulations. For the channels eMJ with "wrong" lepton charge, $eeMJ$, $e\mu MJ$, νeMJ and $\nu\mu MJ$, no mass restriction is imposed, since the SM backgrounds are small.
- The event numbers expected from SM background processes and their systematic uncertainties.
- The signal detection efficiencies (see Table 3) and their uncertainties for all squark decay processes in all selection channels, obtained using the calculated spectrum of sparticle masses.
- The calculated branching ratios of all squark decay modes.

A bound on the squark production cross section σ_{lim} is then obtained from N_{lim}. Sets of model parameters that lead to signal cross sections above σ_{lim} can be excluded.

The case of non-vanishing Yukawa couplings λ'_{131} or λ'_{113}, which correspond to the resonant production of stop

and sbottom squarks, is treated separately since the top and bottom quark masses cannot be neglected in the calculation of couplings and branching ratios. Furthermore, a top quark could be produced in gauge decays. The top quark decays via $t \to bW$, leading to decay products different from those of the first two generations for which the efficiencies are determined. Diagrams which lead to a top in the final state are thus not taken into account in the calculation of the branching ratios. This represents a conservative approach, since most of the top decays are implicitly covered in the selection channels and would be visible in the mass distributions and the total event numbers.

6.2 Limits in the "phenomenological" MSSM

A version of the MSSM is considered here where the masses of the neutralinos, charginos and gluinos, as well as the couplings between any two SUSY particles and a SM fermion/boson, are determined by the usual parameters. These are the "mass" term μ, which mixes the Higgs superfields, the SUSY soft-breaking mass parameters M_1, M_2 and M_3 for $U(1)$, $SU(2)$ and $SU(3)$ gauginos, respectively, and the ratio $\tan\beta$ of the vacuum expectation values of the two neutral scalar Higgs fields. The parameters are defined at the electroweak scale. The gaugino mass terms are assumed to unify at a Grand Unification (GUT) scale to a common value $m_{1/2}$, leading to the usual relations [29] between M_1, M_2 and M_3. The gluino mass is approximated by the value of M_3 at the electroweak scale. The sfermion masses are free parameters in this model. Possible mixing between sfermions is neglected and all squarks are assumed to be degenerate in mass. The possibility of a photino-like χ_1^0 is first discussed, before turning to a complete scan of the SUSY parameter space.

6.2.1 Exclusion limits for a photino-like χ_1^0

For an example set of the MSSM parameters ($\mu = -200\,\text{GeV}$, $M_2 = 80\,\text{GeV}$, $\tan\beta = 2$) leading to a χ_1^0 dominated by its photino component, exclusion limits at the 95 % CL on $\lambda'_{1j1}(j = 1, 2)$ and $\lambda'_{11k}(k = 1, 2)$ are shown in Fig. 7a,b as a function of the squark mass. The full curves represent cases in which sleptons and squarks are assumed to be degenerate in mass. The dashed curves indicate the limits for slepton masses $M_{\tilde{l}}$ fixed at 90 GeV, close to the lowest mass bound from $\not{R}_p$ sfermion searches considering non-vanishing couplings λ' at LEP [4,5]. The HERA sensitivity allows tests of $\not{R}_p$ Yukawa couplings λ' down to around 10^{-2} for squark masses of 100 GeV. For a high squark mass the sensitivity degrades since the production cross section decreases. At a squark mass of 290 GeV, λ'_{1j1} (λ'_{11k}) values larger than 0.6 (0.3) are ruled out.

The branching ratios to all channels calculated for a λ' value exactly at the exclusion limit are illustrated in Figs. 7c–f. The total branching fraction covered exceeds 75 % for all points in the MSSM parameter space and is generally close to 100 %. At large squark masses, a large

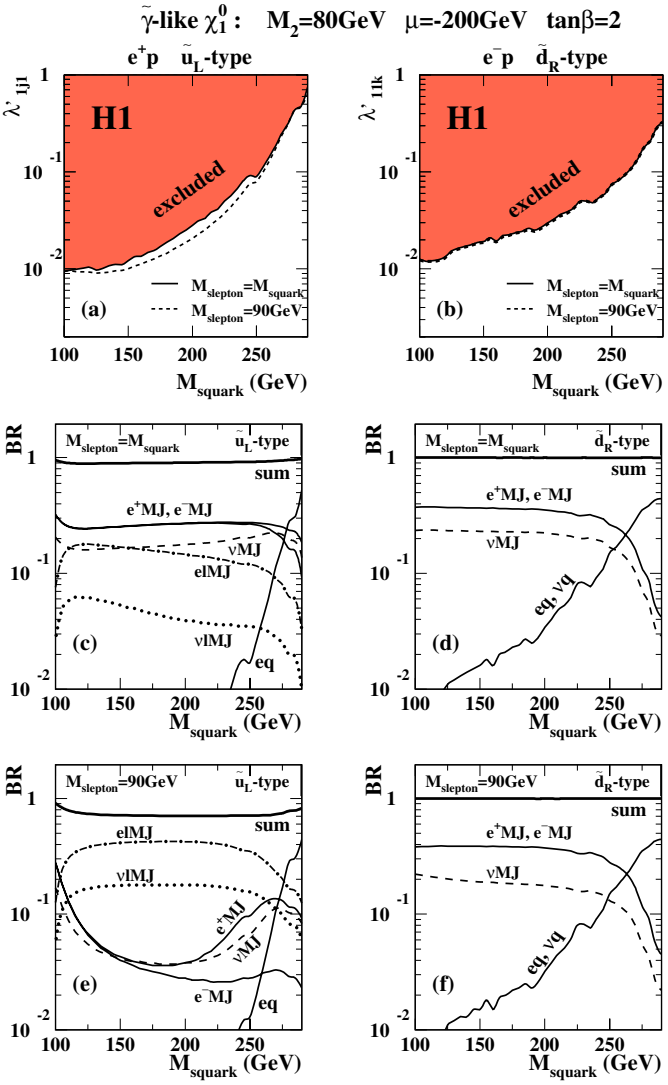

Fig. 7. Exclusion limits at the 95 % CL on **a** λ'_{1j1} with $j = 1, 2$ and **b** λ'_{11k} with $k = 1, 2$. **c**–**f** Branching ratios to the decay channels considered in the analysis for λ' values at the exclusion limits shown in **a** and **b**. The results are shown for MSSM parameters leading to a χ_1^0 dominated by its photino component when slepton and squark masses are assumed to be degenerate **c**, **d** and for a slepton mass of 90 GeV **e**, **f**

Yukawa coupling λ' is necessary to allow visible squark production. As a result the decay channels eq and νq proceeding directly via λ' become important. For smaller masses, the dominant channels in the case of a photino-like χ_1^0 are those with an $e^{\pm}$ and several jets in the final state.

For $\tilde{u}_L$-type squarks ($\lambda'_{1j1} \neq 0$) the relative contributions of the gauge decay channels strongly depend on the slepton mass. In the case of a light slepton ($M_{\tilde{l}} = 90\,\text{GeV}$), the decays of a χ_1^+ into a lepton-slepton pair are kinematically allowed. Thus cascade gauge decays of $\tilde{u}_L$-type squarks are possible, leading to enhanced contributions from the channels $elMJ$ and νlMJ. In contrast, the cascade gauge decays of $\tilde{u}_L$-type squarks are kinematically suppressed for $M_{\tilde{l}} = M_{\tilde{q}}$. The dependence of the λ'_{1j1} limit

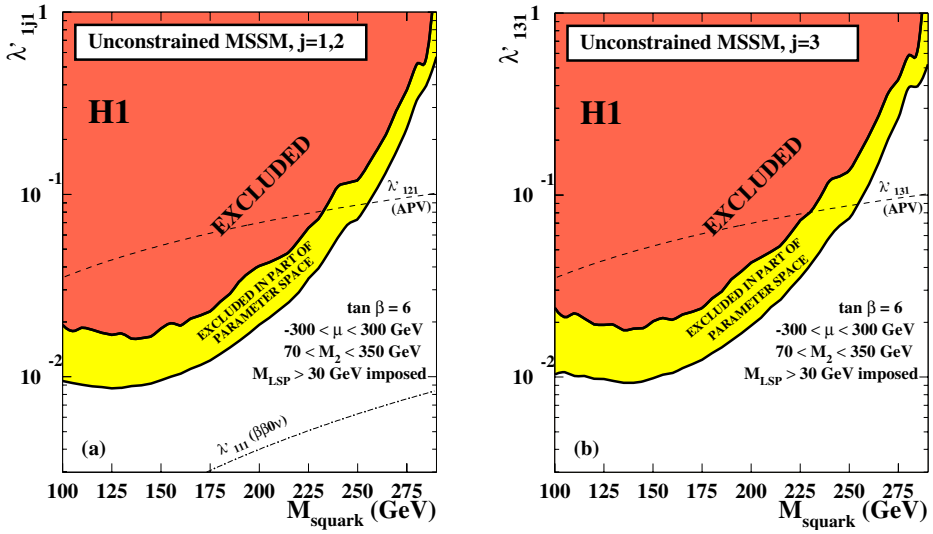

Fig. 8. Exclusion limits (95 % CL) on λ'_{1j1} for **a** $j = 1, 2$ and **b** $j = 3$ as a function of the squark mass from a scan of the MSSM parameter space as indicated in the figures. The two full curves indicate the strongest and the weakest limits on λ' in the parameter space investigated. Indirect limits from neutrinoless double beta decay experiments ($\beta\beta0\nu$) and atomic parity violation (APV) are also shown

on the slepton mass is rather small since the sensitivities of all selection channels are similar. In the case of $\tilde{d}_R$-type squarks ($\lambda'_{11k} \neq 0$), the relative contributions of the decay channels and the resulting limit on λ'_{11k} are almost independent of the slepton mass, since gauge decays of $\tilde{q}_R$ squarks via charginos are suppressed.

The branching ratios to the various decay channels depend on the SUSY parameters. Thus, for parameter values different from those discussed above, different decay channels are dominant. For instance, for a zino-like χ^0_1 the dominant channels at lower squark masses are those with a ν and several jets in the final state [11]. Cascade decays of $\tilde{q}_R$ squarks are also possible for some parameter configurations via gauge decays involving neutralinos or gluinos.

6.2.2 Scan of the parameter space

In order to investigate the dependence of the sensitivity on the MSSM parameters, a scan of M_2 and μ is performed for $\tan\beta = 6$. Again, sleptons are assumed to be degenerate and their mass is set to a fixed value of 90 GeV. Other values for $M_{\tilde{l}}$ and $\tan\beta$ lead to very similar results. The parameters M_2 and μ are varied in the range $70\,\text{GeV} < M_2 < 350\,\text{GeV}$ and $-300\,\text{GeV} < \mu < 300\,\text{GeV}$. Parameter sets leading to a scalar LSP or to LSP masses below 30 GeV are not considered. The latter restriction, as well as the lower value for M_2, are motivated by the exclusion domains resulting from χ searches in $R\!\!\!/_p$ SUSY at LEP [4, 5]. Upper bounds on the couplings λ'_{1j1} and λ'_{11k} are obtained for each point in the (μ, M_2) plane. The results are shown for λ'_{1j1} in Fig. 8 and for λ'_{11k} in Fig. 9. For each plot, the two full curves indicate the strongest and weakest limits obtained for λ' in the parameter space investigated. As can be seen from the narrowness of the region that is excluded in only part of the parameter space, the limits on both λ'_{1j1} and λ'_{11k} are widely independent of the SUSY parameters. For a Yukawa coupling of electromagnetic strength, *i.e.* $\lambda'_{1j1} = \sqrt{4\pi\alpha_{\text{em}}} = 0.3$ ($\lambda'_{11k} = 0.3$), $\tilde{u}_L$, $\tilde{c}_L$ and $\tilde{t}_L$ ($\tilde{d}_R$, $\tilde{s}_R$ and $\tilde{b}_R$) squarks with masses below $\sim 275\,\text{GeV}$ (280 GeV) are excluded at the 95% CL. For a coupling strength smaller by a factor of 100 ($\lambda' = 0.03$), masses up to $\sim 220\,\text{GeV}$ are ruled out.

In Figs. 8 and 9 the results for the direct production of squarks are compared with indirect limits from virtual squark exchange in low energy experiments [30]. The production of $\tilde{u}$ and $\tilde{d}$ squarks via a λ'_{111} coupling is tightly constrained by the non-observation of neutrinoless double beta decay ($\beta\beta0\nu$) [31]. The best indirect limit on the couplings λ'_{121} and λ'_{131} comes from atomic parity violation (APV) measurements [30, 32]. The best indirect limit on the couplings λ'_{112} and λ'_{113} results from tests of charged current universality (CCU) [33]. The HERA results improve the limits on λ' for squarks of the second and third family (*i.e.* $\lambda'_{121}, \lambda'_{131}, \lambda'_{112}, \lambda'_{113}$) for masses up to $\sim 255\,\text{GeV}$.

6.3 Limits in the minimal supergravity model

In this section the minimal Supergravity (mSUGRA) model [34] is considered, where the number of free parameters is reduced by assuming, in addition to the GUT relation between M_1, M_2 and M_3 mentioned previously, a universal mass parameter m_0 for all scalar fields at the GUT scale. By requiring in addition Radiative Electroweak Symmetry Breaking (REWSB) the model is completely determined by m_0, $m_{1/2}$, $\tan\beta$, the sign of μ and the common trilinear coupling at the GUT scale A_0. The modulus of μ is related to the other model parameters. The program SUSPECT 2.1 [35] is used to obtain the

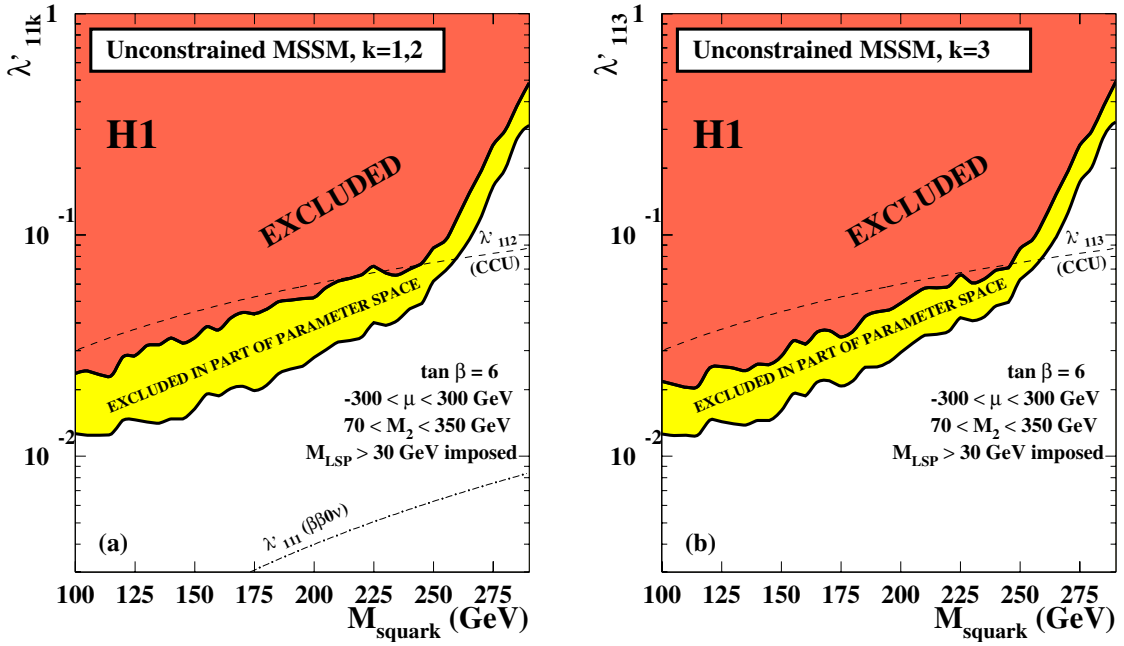

Fig. 9. Exclusion limits (95 % CL) on λ'_{11k} for (**a**) $k = 1, 2$ and (**b**) $k = 3$ as a function of the squark mass from a scan of the MSSM parameter space. The two full curves indicate the strongest and the weakest limits on λ'. Indirect limits from neutrinoless double beta decay experiments ($\beta\beta0\nu$) and tests of charged current universality (CCU) are also shown

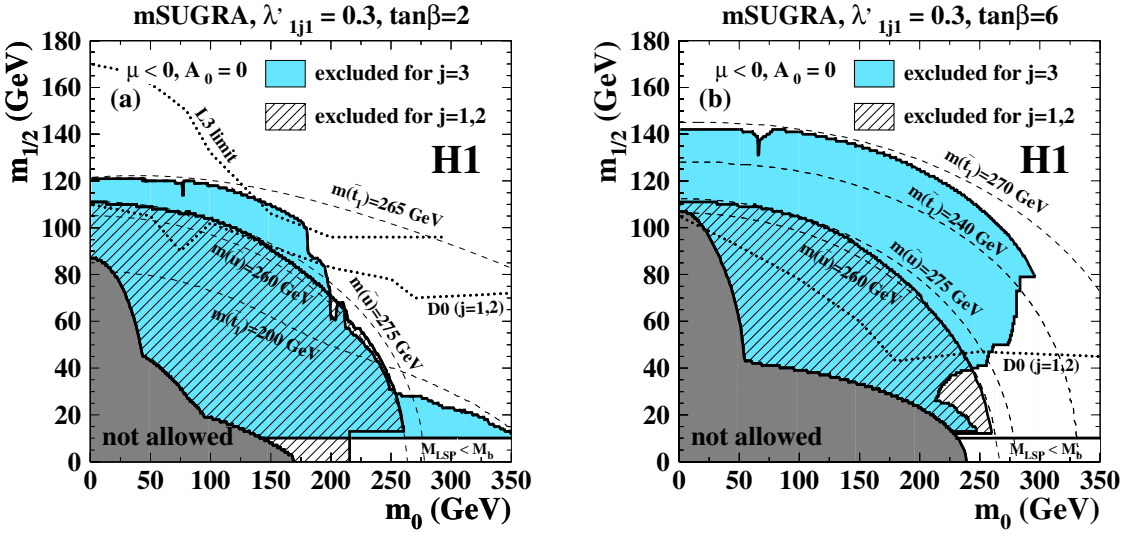

Fig. 10. Excluded regions (95 % CL) in mSUGRA with $\lambda'_{1j1} = 0.3$ for **a** $\tan\beta = 2$ and **b** $\tan\beta = 6$. The region marked "not allowed" corresponds to values of the parameters where no REWSB solution is possible or where the LSP is a sfermion. The dashed lines indicate the curves of constant squark ($\tilde{u}_L$, $\tilde{t}_1$) mass. The limits from LEP and the TeVatron are given by the dotted lines

REWSB solution for $|\mu|$ and calculate the full supersymmetric mass spectrum.

Assuming a fixed value for the $R\!\!\!/_p$ couplings λ'_{1j1} and λ'_{11k}, constraints on the mSUGRA parameters can be set, for example on $(m_0, m_{1/2})$, when $\tan\beta$, A_0, and the sign of μ are fixed. A_0 enters only marginally in the interpretation of physics results at the electroweak scale and it is set to zero. The efficiencies for the detection of all gauge decays of squarks involving a gaugino lighter than 30 GeV are set to zero since the parameterisation of the efficiencies is not valid in this domain. The corresponding parameter space is already excluded by χ searches in $R\!\!\!/_p$ SUSY at LEP [4,5].

6.3.1 Results for the first and second families

For $\mu < 0$, the exclusion limits at the 95 % CL obtained for a Yukawa coupling $\lambda'_{1j1} = 0.3$ ($j = 1, 2$) in the $(m_0, m_{1/2})$ plane are shown by the hatched histograms in Fig. 10 for the two example values (a) $\tan\beta = 2$ and (b) $\tan\beta = 6$.

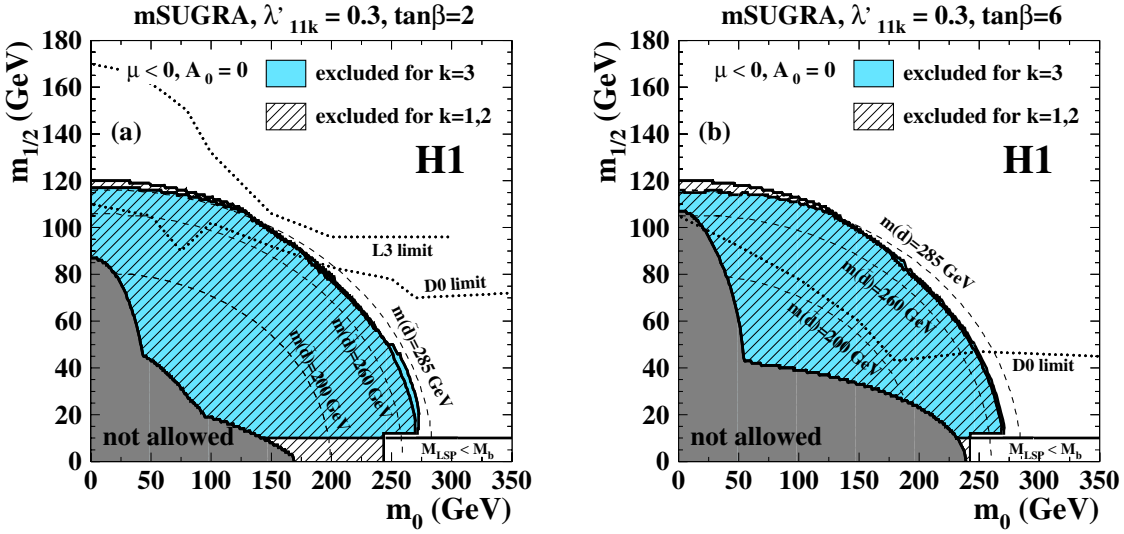

Fig. 11. Excluded regions (95 % CL) in mSUGRA with $\lambda'_{11k} = 0.3$ for **a** $\tan\beta = 2$ and **b** $\tan\beta = 6$. The region marked "not allowed" corresponds to values of the parameters where no REWSB solution is possible or where the LSP is a sfermion. The dashed lines indicate the curves of constant squark mass. The limits from LEP and the TeVatron are given by the dotted lines

The corresponding results for $\lambda'_{11k} = 0.3$ ($k = 1, 2$) are shown in Fig. 11. The domains marked "not allowed" correspond to parameter values where no REWSB solution is possible or where the LSP is a sfermion.

The constraints on $(m_0, m_{1/2})$ are very similar for both values of $\tan\beta$ and both $R\!\!\!/_p$ coupling types, λ'_{1j1} and λ'_{11k}, since the mixing of the squark states is very small for $j = 1, 2$ and $k = 1, 2$. The excluded regions approximately follow curves of constant squark mass. For $\lambda'_{1j1} = 0.3$, the parameter space defined by $M_{\tilde{q}} < 275\,\mathrm{GeV}$ is nearly fully excluded. For $\lambda'_{11k} = 0.3$, the squark mass limit is slightly higher, $M_{\tilde{q}} < 285\,\mathrm{GeV}$, because of the higher squark production cross section in $e^- p$ collisions for equal couplings.

The results of the searches for $R\!\!\!/_p$ SUSY by the D0 experiment [7] at the TeVatron, which exploit di-electron events, are also shown in Figs. 10 and 11. For $\tan\beta = 2$, the H1 limits are more stringent only for low values of m_0, whereas for $\tan\beta = 6$ the domain excluded by H1 extends considerably beyond the region ruled out by the D0 experiment. For $\tan\beta = 2$, the parameter space is more strongly constrained by the searches for χ's and sleptons at the L3 experiment [5] at LEP, as shown in Figs. 10 and 11. This is the largest $\tan\beta$ value considered in [5]. Results for higher values are expected to be similar. The LEP and TeVatron limits are independent of the Yukawa coupling.

6.3.2 Results on stop and sbottom production

A non-vanishing coupling λ'_{131} would lead to the production of a stop squark. The weak stop eigenstates $\tilde{t}_L$ and $\tilde{t}_R$ mix through an angle $\theta_{\tilde{t}}$ to form the mass eigenstates $\tilde{t}_1 = \cos\theta_{\tilde{t}}\,\tilde{t}_L + \sin\theta_{\tilde{t}}\,\tilde{t}_R$ and $\tilde{t}_2 = -\sin\theta_{\tilde{t}}\,\tilde{t}_L + \cos\theta_{\tilde{t}}\,\tilde{t}_R$, whose production cross sections scale as $\lambda'^2_{131}\cos^2\theta_{\tilde{t}}$ and $\lambda'^2_{131}\sin^2\theta_{\tilde{t}}$, respectively. Thus the lighter state $\tilde{t}_1$ does not necessarily have the largest production cross section. Similarly, for a non-vanishing λ'_{113}, sbottom production could be possible. The weak sbottom states $\tilde{b}_L$ and $\tilde{b}_R$ mix to form the mass eigenstates $\tilde{b}_1 = \cos\theta_{\tilde{b}}\,\tilde{b}_L + \sin\theta_{\tilde{b}}\,\tilde{b}_R$ and $\tilde{b}_2 = -\sin\theta_{\tilde{b}}\,\tilde{b}_L + \cos\theta_{\tilde{b}}\,\tilde{b}_R$ and the production cross section for $\tilde{b}_1$ ($\tilde{b}_2$) scales as $\lambda'^2_{113}\sin^2\theta_{\tilde{b}}$ ($\lambda'^2_{113}\cos^2\theta_{\tilde{b}}$). The treatment of stop production is described in the following. Sbottom mixing is treated in the same way.

For the selection channels where the signal is integrated over the whole mass range, the fraction of the visible signal in a given selection channel k, is $\sum_{i=1,2}(\varepsilon\beta)_{k,i}\sigma_i/\sigma_{\mathrm{tot}}$, where $(\varepsilon\beta)_{k,i}$ is the total visible branching ratio[6] of the selection channel k for the state $\tilde{t}_i$, σ_i is the production cross section of $\tilde{t}_i$ and $\sigma_{\mathrm{tot}} = \sigma_1 + \sigma_2$ is the total signal cross section. For the channels in which the signal is integrated over a mass bin only the contribution of the state $\tilde{t}_i$ for which the sensitivity is maximal, *i.e.* for which $\sigma_i(\sum_k(\beta\varepsilon)_{k,i})$ is maximal, is taken into account in the above summation. The numbers of observed and expected events are then integrated in the mass bin corresponding to $\tilde{t}_i$ only.

Using this procedure for both the stop and the sbottom case, exclusion limits are derived for $A_0 = 0$ and $\mu < 0$ for $\tan\beta = 2$ and $\tan\beta = 6$. The excluded regions in the $(m_0, m_{1/2})$ plane for $\lambda'_{131} = 0.3$ and $\lambda'_{113} = 0.3$ are shown in Figs. 10 and 11, respectively. The domain below the line $m_{1/2} \simeq 10\,\mathrm{GeV}$ is not considered since it corresponds to cases where the only possible LSP decay, into $\nu b\bar{d}$, is kinematically forbidden.

In the case of stop production for $\tan\beta = 2$, shown in Fig. 10a, the excluded domain is slightly larger than that

[6] The total visible branching ratio $(\varepsilon\beta)_k$ of a selection channel k is given by $(\varepsilon\beta)_k = \sum_j \varepsilon_{k,j}\beta_j$, where β_j is the branching ratio of the squark decay mode j and $\varepsilon_{k,j}$ is the corresponding efficiency in the selection channel k. The sum runs over all decay modes j considered in the selection channel.

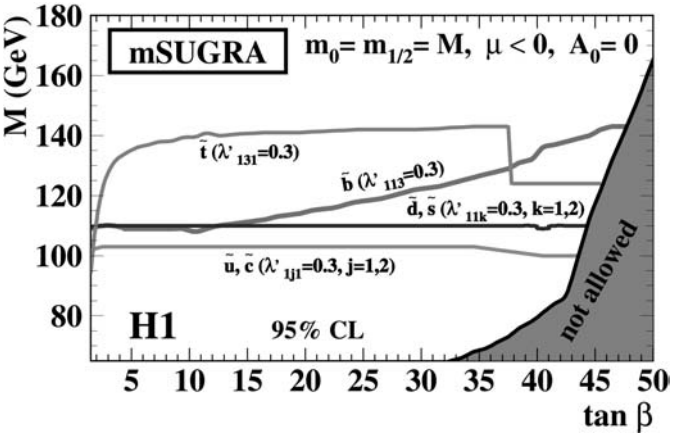

Fig. 12. Exclusion limits for $m_0 = m_{1/2} = M$ in mSUGRA as a function of $\tan\beta$. The 95 % CL exclusion limits for $\lambda'_{1jk} = 0.3$ are shown. The areas below the curves are excluded. The region marked "not allowed" corresponds to values of the parameters where no REWSB solution is possible or where the LSP is a sfermion

ruled out previously for $\lambda'_{1j1} = 0.3$ ($j = 1, 2$) due to the mixing in the stop sector which leads to $\tilde{t}_1$ masses smaller than the masses of the other squarks. Consequently, larger values of $m_{1/2}$ and m_0 can be probed. As shown in Fig. 10b this remains the case for $\tan\beta = 6$ as long as $m_{1/2}$ is large enough to ensure that the mass of the lightest neutralino is above 30 GeV. When the χ_1^0 becomes too light, the detection efficiencies for the channels involving a χ_1^0 (in particular the process $\chi_1^+ \to \chi_1^0$) are set to zero and the sensitivity is only through the eq channel or the decays $\tilde{t} \to b\chi_1^+$ followed by a $\not{R}_p$ decay of the chargino. For even smaller $m_{1/2}$, if the χ_1^+ mass is below 30 GeV, only the eq channel contributes. For $\tan\beta = 2$ ($\tan\beta = 6$), $\tilde{t}_1$ masses up to 265 GeV (270 GeV) can be excluded for $\lambda'_{131} = 0.3$. These masses are smaller than the maximal sensitivity reached for the same coupling value for $j = 1, 2$ because of the $\cos^2\theta_{\tilde{t}}$ reduction of the $\tilde{t}_1$ cross section. For $\tan\beta = 2$, the limits obtained from this analysis are comparable to the LEP sensitivity in χ and slepton searches at intermediate values of m_0. In the same part of the parameter space, the H1 limits for higher values of $\tan\beta$ extend considerably beyond the LEP sensitivity which is expected to be similar to that for $\tan\beta = 2$.

In the case of sbottom production (Fig. 11) the limits are similar to those obtained for $k = 1, 2$, since the mixing in the sbottom sector is small at the $\tan\beta$ values considered. Thus, the mass difference between $\tilde{b}_1$ and $\tilde{b}_2$ is small. The sensitivity follows curves of equal $\tilde{b}_2$ masses because the production cross section for this state is much higher than for $\tilde{b}_1$ if the mixing angle is small. The parameter space leading to $\tilde{b}_2$ masses up to 285 GeV is ruled out.

6.3.3 Dependence of the results on $\tan\beta$

In order to extend the parameter space to larger values of $\tan\beta$, a scan of this parameter is carried out. The number of free parameters is reduced by setting the masses m_0 and $m_{1/2}$ to a common value M. The 95 % CL limits on M are shown in Fig. 12 as a function of $\tan\beta$ for $\lambda'_{1jk} = 0.3$. All squark flavours are considered. For the first two families the exclusion curves are rather flat since mixing effects are very small. Assuming equal $\not{R}_p$ couplings, a larger part of the parameter space is excluded for $\tilde{d}$ and $\tilde{s}$ production than for $\tilde{u}$ and $\tilde{c}$ production because of the higher squark production cross section in e^-p collisions. For squarks of the third family, mixing effects become important. For $\tan\beta \gtrsim 10$ the increase of the mixing angle $\theta_{\tilde{b}}$ results in an improvement of the sbottom limit since it leads to a smaller $\tilde{b}_1$ mass, giving a higher $\tilde{b}_1$ production cross section. The mixing effects are largest in the stop sector, leading to more stringent limits on M. For very low values of $\tan\beta$, the $\cos^2\theta_{\tilde{t}}$ reduction of the $\tilde{t}_1$ production cross section is important. At values of $\tan\beta \gtrsim 37$, the mixing of the two stau ($\tilde{\tau}$) states leads to decay chains involving light $\tilde{\tau}$s which result in final states including τ leptons. These channels are not searched for explicitly. Thus, in this region of the parameter space, the limit on stop production becomes less restrictive.

7 Conclusion

A search for the $\not{R}_p$ production of squarks in e^+p and e^-p collisions at HERA has been presented. No significant deviation from the SM is observed in any of the final state topologies resulting from direct or indirect R_p violating squark decays. Mass dependent limits on the $\not{R}_p$ couplings λ'_{1jk} are derived within a phenomenological version of the MSSM. The existence of $\tilde{u}_L$-type and $\tilde{d}_R$-type squarks of all three generations with masses up to 275 GeV and 280 GeV, respectively, is excluded at the 95% CL, for a Yukawa coupling equal to $\sqrt{4\pi\alpha_{\rm em}}$, in a large part of the MSSM parameter space. These mass limits extend considerably beyond the reach of other collider experiments. For lower squark masses, the results improve the indirect bounds set by low-energy experiments. Exclusion limits are also derived in the more restricted mSUGRA model, for which the limits obtained are competitive with and complementary to those derived at the LEP and TeVatron colliders.

Acknowledgements. We are grateful to the HERA machine group whose outstanding efforts have made this experiment possible. We thank the engineers and technicians for their work in constructing and now maintaining the H1 detector, our funding agencies for financial support, the DESY technical staff for continual assistance and the DESY directorate for support and for the hospitality which they extend to the non-DESY members of the collaboration.

References

1. C. Adloff et al. [H1 Collaboration], Eur. Phys. J. C **20**, 639 (2001) [hep-ex/0102050]

2. T. Ahmed et al. [H1 Collaboration], Z. Phys. C **64**, 545 (1994)
3. A. Heister et al. [ALEPH Collaboration], Eur. Phys. J. C **25**, 1 (2002) [hep-ex/0201013]; P. Abreu et al. [DELPHI Collaboration], Phys. Lett. B **502**, 24 (2001) [hep-ex/0102045]; P. Abreu et al. [DELPHI Collaboration], Phys. Lett. B **500**, 22 (2001) [hep-ex/0103015]; P. Abreu et al. [DELPHI Collaboration], Phys. Lett. B **487**, 36 (2000) [hep-ex/0103006]; P. Achard et al. [L3 Collaboration], Phys. Lett. B **524**, 65 (2002) [hep-ex/0110057]
4. A. Heister et al. [ALEPH Collaboration], Eur. Phys. J. C **31**, 1 (2003) [hep-ex/0210014]; G. Abbiendi *et al.* [OPAL Collaboration], CERN-EP-2003-036, accepted by Eur. Phys. J. C [hep-ex/0310054]; G. Abbiendi et al. [OPAL Collaboration], Eur. Phys. J. C **11**, 619 (1999) [hep-ex/9901037]
5. M. Acciarri et al. [L3 Collaboration], Eur. Phys. J. C **19**, 397 (2001) [hep-ex/0011087]
6. D. Acosta et al. [CDF Collaboration], Phys. Rev. Lett. **92**, 051803 (2004) [hep-ex/0305010]; F. Abe *et al.* [CDF Collaboration], Phys. Rev. Lett. **83**, 2133 (1999) [hep-ex/9908063]; V. M. Abazov et al. [D0 Collaboration], Phys. Rev. Lett. **89**, 261801 (2002) [hep-ex/0207100]; V.M. Abazov *et al.* [D0 Collaboration], Phys. Rev. Lett. **89**, 171801 (2002) [hep-ex/0111053]; B. Abbott et al. [D0 Collaboration], Phys. Rev. **D62**, 071701 (2000) [hep-ex/0005034]
7. B. Abbott et al. [D0 Collaboration], Phys. Rev. Lett. **83**, 4476 (1999) [hep-ex/9907019]
8. J. Butterworth, H. Dreiner, Nucl. Phys. B **397**, 3 (1993) and references therein
9. W. Buchmüller, R. Rückl, D. Wyler, Phys. Lett. B **191**, 442 (1987); *Erratum* Phys. Lett. B **448**, 320 (1999)
10. T. Plehn, H. Spiesberger, M. Spira, P.M. Zerwas, Z. Phys. C **74**, (1997) 611 [hep-ph/9703433]
11. J. Haller, "Search for Squark Production in *R*-Parity Violating Supersymmetry at HERA", Ph.D. Thesis, University of Heidelberg, Germany, October 2003, DESY-THESIS-2003-035 (available at http://www-h1.desy.de/psfiles/theses/h1th-318.ps)
12. I. Abt et al. [H1 Collaboration], Nucl. Instrum. Meth. A **386**, 310 and 348 (1997)
13. B. Andrieu et al. [H1 Calorimeter Group], Nucl. Instrum. Meth. A **336**, 460 (1993)
14. B. Andrieu et al. [H1 Calorimeter Group], Nucl. Instrum. Meth. A **350**, 57 (1994); B. Andrieu et al. [H1 Calorimeter Group], Nucl. Instrum. Meth. A **336**, 499 (1993)
15. DJANGO 6.2; G.A. Schuler, H. Spiesberger, Proc. of the Workshop Physics at HERA, W. Buchmüller, G. Ingelman (eds.) (October 1991, DESY-Hamburg) Vol. 3 p. 1419
16. L. Lönnblad, Comput. Phys. Commun. **71**, 15 (1992)
17. G. Gustafson, U. Pettersson, Nucl. Phys. B **306**, 746 (1988); *idem*, *addendum* Lund University preprint LU-TP-87-19, (October 1987) 4; B. Andersson, G. Gustafson, L. Lönnblad, U. Pettersson, Z. Phys. C **43**, 625 (1989)
18. H. Jung, Comput. Phys. Commun. **86**, 147 (1995)
19. V.N. Gribov, L. N. Lipatov, Sov. J. Nucl. Phys. **15**, 438 (1972); G. Altarelli, G. Parisi, Nucl. Phys. B **126**, 298 (1977); Y.L. Dokshitzer, Sov. Phys. JETP **46**, 641 (1977)
20. H.-L. Lai et al., Eur. Phys. J. C **12**, 375 (2000) [hep-ph/9903282]
21. T. Sjöstrand, Lund Univ. preprint LU-TP-95-20 (August 1995) 321 pp.;
idem, CERN TH-7112 (1993) [hep-ph/9508391]
22. PYTHIA 5.7; T. Sjöstrand, CERN-TH-6488 (1992); T. Sjöstrand, Comput. Phys. Commun. **82**, 74 (1994)
23. U. Baur, J.A. Vermaseren, D. Zeppenfeld, Nucl. Phys. B **375**, 3 (1992)
24. LEGO 0.02; K. Rosenbauer, Ph.D. thesis, RWTH Aachen (in German), PITHA 95/16 (July 1995)
25. S. Katsanevas, P. Morawitz, Comput. Phys. Commun. **112**, 227 (1998) [hep-ph/9711417]; N. Ghodbane, S. Katsanevas, P. Morawitz, E. Perez, SUSYGEN 3, [hep-ph/9909499]
26. A. Blondel, F. Jacquet, Proceedings of the Study of an *ep* Facility for Europe, ed. U. Amaldi, DESY report 79-48, 391 (1979)
27. C. Adloff et al. [H1 Collaboration], Eur. Phys. J. C **30**, 1 (2003) [hep-ex/0304003]
28. T. Junk, Nucl. Instrum. Meth. A **434**, 435 (1999) [hep-ex/9902006]
29. H.P. Nilles, Phys. Rept. **110**, 1 (1984); H.E. Haber and G.L. Kane, Phys. Rept. **117**, 75 (1985)
30. H. Dreiner, published in "Perspectives on Supersymmetry", Ed. G.L. Kane, World Scientific, 462 (1997) [hep-ph/9707435]
31. R.N. Mohapatra, Phys. Rev. D **D34**, 3457 (1986); J.D. Vergados, Phys. Lett. B **184**, 55 (1987); M. Hirsch, H.V. Klapdor-Kleingrothaus, S.G. Kovalenko, Phys. Lett. B **352**, 1 (1995) [hep-ph/9502315]; M. Hirsch, H.V. Klapdor-Kleingrothaus, S.G. Kovalenko, Phys. Rev. Lett. **75**, 17 (1995); M. Hirsch, H.V. Klapdor-Kleingrothaus, S.G. Kovalenko, Phys. Rev. D **53**, 1329 (1996) [hep-ph/9502385]
32. P. Langacker, Phys. Lett. B **256**, 277 (1991)
33. V. Barger, G.F. Giudice, T. Han, Phys. Rev. D **40**, 2987 (1989)
34. M. Drees, M.M. Nojiri, Nucl. Phys. B **369**, 54 (1992); H. Baer, X. Tata, Phys. Rev. D **47**, 2739 (1993); G.L. Kane, C. Kolda, L. Roszkowski, J.D. Wells, Phys. Rev. D **49**, 6173 (1994)
35. A. Djouadi, J.L. Kneur, G. Moultaka, SUSPECT 2.1, [hep-ph/0211331]